Electrochimica Acta 131 (2014) 214–227

Contents lists available at ScienceDirect

Electrochimica Acta

journal homepage: www.elsevier.com/locate/electacta

Electrochemical Impedance of a Battery Electrode with Anisotropic Active Particles

Juhyun Song[a,2], Martin Z. Bazant[a,b,*,1]

[a] Department of Chemical Engineering, Massachusetts Institute of Technology, 77 Massachusetts Avenue, Cambridge, Massachusetts 02139, United States
[b] Department of Mathematics, Massachusetts Institute of Technology, 77 Massachusetts Avenue, Cambridge, Massachusetts 02139, United States

ARTICLE INFO

Article history:
Received 15 September 2013
Received in revised form 4 February 2014
Accepted 7 March 2014
Available online 21 March 2014

Keywords:
anisotropic active material
impedance spectroscopy
battery electrode
regular perturbation analysis
finite Fourier transformation

ABSTRACT

Electrochemical impedance spectra for battery electrodes are usually interpreted using models that assume isotropic active particles, having uniform current density and symmetric diffusivities. While this can be reasonable for amorphous or polycrystalline materials with randomly oriented grains, modern electrode materials increasingly consist of highly anisotropic, single-crystalline, nanoparticles, with different impedance characteristics. In this paper, analytical expressions are derived for the impedance of anisotropic particles with tensorial diffusivities and orientation-dependent surface reaction rates and capacitances. The resulting impedance spectrum contains clear signatures of the anisotropic material properties and aspect ratio, as well as statistical variations in any of these parameters.

1. Introduction

Electrochemical impedance spectroscopy (EIS) is used in various fields, such as energy storage and conversion [1–6], cell biology [7,8], corrosion science [9,10], and catalysis [11,12], to characterize transport, reaction, and accumulation of charge carriers in the systems. For insertion battery electrodes, it has also been widely used across many different material compositions [1–3]. Various models have been introduced to interpret the battery impedance behavior. After adopting the Randles model for combined contribution of charge accumulation, insertion reaction, and transport in active material [13,14], models were further developed to consider different particle shape [15,16], size distribution [16–19], phase transformation [20,21], and additional layers on the active particles [17,22,23]. Some also incorporate the concentration gradient along the thickness of a porous electrode [17,23,24] and its heterogeneous thickness [18,19,25]. Nevertheless, essentially all models assume isotropic properties for the active particles, regardless of their area of application.

In contrast, most battery materials currently under investigation are strongly anisotropic, which means that behavior of charge carriers in the materials varies with the direction in respect to the crystallographic axes [26–32]. The anisotropy is attributed to different activation barriers along the hopping paths of charge carriers depending on the direction. Since many battery materials have high electron mobility compared to that of ions [15,27], it is the ion hopping that determines the anisotropy in transport of charge carriers as well as in surface insertion kinetics [15,33,34]. For example, Li_xCoO_2 has a layered metal oxide structure, where lithium ions can move quickly through the plane between the metal oxide layers, but their movement across the layers is less likely and very slow [28,29]. On the other hand, Li_xFePO_4 has an olivine structure, where lithium ions can move quickly through one-dimensional channels in the *b*-crystallographic direction [30–32]. Models also predict that intercalation kinetics [35], phase separation dynamics [36], and nucleation [37] are highly anisotropic due to tensorial coherency strain and different composition-dependent surface on each crystal facet [38,39]. Like Li_xFePO_4, other important battery materials tend to phase-separate when they are alloying with Li ions [40–42], and their impedance characteristics are beginning to be considered [20,21]. In this paper, however, we confine our scope to the materials forming a single phase solid solution. This also includes materials that tend to phase-separate, such as $Li_xMn_2O_4$ and Li_xFePO_4, while outside of their miscibility gaps for $x \approx 0$ or $x \approx 1$.

Isotropic models of active particles are still widely employed in EIS studies of batteries, in part because traditional active particles were large enough to have many randomly oriented crystal

* Corresponding author.
E-mail address: bazant@mit.edu (M.Z. Bazant).
[1] ISE member
[2] Current address: Samsung Cheil Industries Inc., 332-2 Gocheon-dong, Uiwang, Gyunggi 437-711, South Korea

http://dx.doi.org/10.1016/j.electacta.2014.03.013
0013-4686/

Nomenclature

A_p	particle surface area
c	local ion concentration
c_s	surface ion concentration
$(\nabla c)_s$	ion concentration gradient at surface
$\hat{\tilde{c}}$	$= \left(-\partial\Delta\phi_{eq}/\partial c\right)\hat{c}/\Delta\hat{\phi}$, dimensionless local ion concentration
C_p	particle surface capacitance
C_{surf}	surface capacitance
$C_{surf,x}$	$=C_{surf}(\mathbf{e}_x)$, surface capacitance on x normal surface
$C_{surf,y}$	$=C_{surf}(\mathbf{e}_y)$, surface capacitance on y normal surface
$\mathbf{D}_{ch}$	chemical diffusivity tensor
$D_{ch,x}$	chemical diffusivity in x direction
$D_{ch,y}$	chemical diffusivity in y direction
$D_{ch,z}$	chemical diffusivity in z direction
e	elementary electric charge
$\mathbf{e}_x$	unit vector in x direction
$\mathbf{e}_y$	unit vector in y direction
i	$=\sqrt{-1}$, unit imaginary number
j_0	exchange current density
j_{acc}	accumulation current density
j_{ins}	insertion current density
j_{tot}	total current density
J_p	total current on particle surface
J_{ov}	overall electrode current
k	Boltzmann's constant
l_x	one half of particle length in x direction
l_y	one half of particle length in y direction
$\tilde{l}_x$	$= l_x/\bar{L}_x$, dimensionless particle length in x direction
$\tilde{l}_y$	$= l_y/\bar{L}_y$, dimensionless particle length in y direction
L_x	one half of particle length in x direction, a random variable
L_y	one half of particle length in y direction, a random variable
$\bar{L}_x$	mean value of L_x
$\bar{L}_y$	mean value of L_y
$\tilde{L}_x$	$= L_x/\bar{L}_x$, dimensionless particle length in x direction, a random variable
$\tilde{L}_y$	$= L_y/\bar{L}_y$, dimensionless particle length in y direction, a random variable
$\mathbf{n}$	surface normal vector
n_p	index of summation for active particles
N_p	total number of active particles
$Pr_{\mathbf{V}_d}$	joint probability density function of $\mathbf{V}_d$
$Pr_{\tilde{L}x,\tilde{L}y}$	joint probability density function of $\tilde{L}_x$ and $\tilde{L}_y$
R_p	particle surface resistance
t	time variable
T	temperature
$\mathbf{v}_d$	vector of distributed parameters, a realization
$\mathbf{V}_d$	vector of distributed parameters, a random vector variable
x	spatial variable in x direction
$\tilde{x}$	$= x/l_x$, dimensionless spatial variable in x direction
X	arbitrary variable
X_0	reference state response in X
X_1	ε-order perturbation in X
$\hat{X}$	Fourier coefficient of perturbation in X
y	spatial variable in y direction
$\tilde{y}$	$= y/l_y$, dimensionless spatial variable in y direction
z_{acc}	local accumulation impedance
z_D	local diffusion impedance
z_G	local Gerischer impedance
z_{ins}	local insertion impedance
z_{tot}	local total impedance
Z_p	particle impedance
Z_{ov}	overall electrode impedance
$\tilde{z}_{tot}$	$= z_{tot}/\rho_{ct,x}$, dimensionless local total impedance
$\tilde{Z}_p$	$= 8l_yZ_p/\rho_{ct,x}$, dimensionless particle impedance
$\tilde{Z}_{p,G}$	Gerischer limit of dimensionless particle impedance
$\tilde{Z}_{ov}$	$= 8\bar{L}_yN_pZ_{ov}/\rho_{ct,x}$, dimensionless overall electrode impedance

Greek letters

α	charge transfer coefficient
β_x	$= \rho_{D,x}/\rho_{ct,x}$, ratio of diffusion characteristic resistance in x direction and charge transfer resistance on x normal surface
β_y	$= \rho_{D,y}/\rho_{ct,y}$, ratio of diffusion characteristic frequency in y direction and charge transfer resistance on y normal surface
χ_x	$= \omega_{RC,x}/\omega_{D,x}$, ratio of RC characteristic frequency on x normal surface and diffusion characteristic frequency in x direction
χ_y	$= \omega_{RC,y}/\omega_{D,y}$, ratio of RC characteristic frequency on y normal surface and diffusion characteristic frequency in y direction
ε	arbitrary small number
$\Delta\phi$	potential drop across electrolyte/active material interface
$\Delta\phi_{eq}$	equilibrium potential drop of insertion reaction
$-\partial\Delta\phi_{eq}/\partial c$	Nernst shift coefficient
γ	$= l_x/l_y$, geometric aspect ratio of a rectangular particle
η	surface overpotential
ν	$= \rho_{ct,y}/\rho_{ct,x}$, ratio of charge transfer resistances
ρ_{xy}	correlation between $\tilde{L}_x$ and $\tilde{L}_y$
ρ_{ct}	$= kT/j_0e$, charge transfer resistance
$\rho_{ct,x}$	$= \rho_{ct}(\mathbf{e}_x)$, charge transfer resistance on x normal surface
$\rho_{ct,y}$	$= \rho_{ct}\left(\mathbf{e}_y\right)$, charge transfer resistance on y normal surface
$\rho_{D,x}$	$= \left(-\partial\Delta\phi_{eq}/\partial c\right)l_x/eD_{ch,x}$, diffusion characteristic resistance in x direction
$\rho_{D,y}$	$= \left(-\partial\Delta\phi_{eq}/\partial c\right)l_y/eD_{ch,y}$, diffusion characteristic resistance in y direction
Σ_{xx}	variance in $\tilde{L}_x$
Σ_{yy}	variance in $\tilde{L}_y$
Σ_{xy}, Σ_{yx}	covariance of $\tilde{L}_x$ and $\tilde{L}_y$
τ	$= \omega_{D,y}/\omega_{D,x}$, ratio of diffusion characteristic frequencies
ω	applied frequency
$\omega_{D,x}$	$= D_{ch,x}/l_x^2$, diffusion characteristic frequency in x direction
$\omega_{D,y}$	$= D_{ch,y}/l_y^2$, diffusion characteristic frequency in y direction
$\omega_{RC,p}$	RC characteristic frequency of particle impedance
$\omega_{RC,x}$	$= \left(\rho_{ct,x}C_{surf,x}\right)^{-1}$, RC characteristic frequency on x normal surface
$\omega_{RC,y}$	$= \left(\rho_{ct,y}C_{surf,y}\right)^{-1}$, RC characteristic frequency on y normal surface
$\tilde{\omega}$	$= \omega/\omega_{D,x}$, dimensionless applied frequency
$\mathbf{\Omega}$	domain of $\mathbf{V}_d$

grains and presented lumped isotropic behaviors [43]. Meanwhile, with the recent developments in synthesis of active materials, modern battery electrodes are made of small particles with a few grains or even a single grain, to achieve excellent rate capability and long cycle life [44–47]. Then, the anisotropic particle properties may significantly affect their impedance spectra, and this motivates us to consider the effects of particle anisotropies on battery impedance. Therefore in this study, we first illustrate a generic approach to arrive at an impedance model for a battery electrode with anisotropic active particles. Using the generic framework, we then analytically study the impedance of an anisotropic 2D rectangular particle, where we could investigate the effects of anisotropies in diffusion, surface kinetics, and surface capacitance. Lastly, we study the overall impedance of an electrode where the particles have anisotropic distributions in length scales. Throughout this work, we assumed that the active material has high electron mobility and forms a homogeneous solid solution. It is also assumed for a porous electrode that its thickness is nominal and the electrolyte conductivity is high so that the models do not account for any gradient that may develop along the electrode thickness.

2. General Theory

Impedance is measured by applying a small perturbation, either in potential or current, to an electrochemical system around a reference state and measuring the response in the other variable [48]. When a system is approximated linear and perturbed by a small sinusoidal stimulus, relevant variables fluctuate correspondingly in isofrequential sinusoidal forms with negligible harmonic responses. Applying a regular perturbation analysis, an arbitrary system variable, X, can be expanded as a power series of a sufficiently small parameter, ε, where the zero-order term and the ε-order term represent the reference state response and the sinusoidal perturbation, respectively. The higher-order terms, represented by the mathematical order of ε^2, correspond to the non-linear harmonic responses, which are relatively small.

$$X = X_0 + \varepsilon X_1 + O\left(\varepsilon^2\right) = X_0 + \varepsilon \hat{X} \exp(i\omega t) + O\left(\varepsilon^2\right) \tag{1}$$

where $i = \sqrt{-1}$ is the unit imaginary number, ω is the applied frequency, and t is the time variable. The Fourier transform of the perturbation term, X_1, yields $\hat{X}$, the Fourier coefficient, which is a complex number containing information related to the magnitude and the phase of the perturbation in X.

2.1. Anisotropic transport of charge carriers

The system under initial investigation is a single crystal nanoparticle of anisotropic battery material, in which diffusivities of charge carriers vary depending on the diffusion direction. The system is fully exposed to electrolyte solution, except small contacts to electron conducting material. Ions intercalate into the system from the interface with electrolyte solution, and electrons come from the contacts with conducting material. In many battery materials, the mobility of electrons is much higher than that of ions [15,27]. Under such conditions, the neutral diffusion of ions limits the solid-state transport of charge carriers, and the Fick's neutral diffusion equation can be recovered in its tensor form, to describe the anisotropic ion transport in the system.

$$\frac{\partial c}{\partial t} = \nabla \cdot (\boldsymbol{D}_{ch} \nabla c) \tag{2}$$

where c is the local ion concentration, and $\mathbf{D}_{ch}$ is the chemical diffusivity tensor. It is always possible to make $\mathbf{D}_{ch}$ diagonal by setting the coordinate axes aligned with the diffusion principal axes.

$$\mathbf{D}_{ch} = \begin{pmatrix} D_{ch,x} & 0 & 0 \\ 0 & D_{ch,y} & 0 \\ 0 & 0 & D_{ch,z} \end{pmatrix} \tag{3}$$

Each component of $\mathbf{D}_{ch}$ is the diffusivity in corresponding direction and may be different from the others. For olivine structure as an example, $D_{ch,y}$ is much larger than the two others, and Li ions have effectively 1D transport in y or (0 1 0) direction [27,30]. Calculation of the ion diffusivities in battery materials has been extensively studied in the community using the first principle approaches [27,29,30,49], and it has also been shown that the anisotropy in diffusion depends on the system size [31].

In calculation of impedance, the anisotropic diffusion equation is expanded by substituting the power series expression in Equation (1):

$$\frac{\partial c_0}{\partial t} + \varepsilon \frac{\partial c_1}{\partial t} + O\left(\varepsilon^2\right) = \nabla \cdot \left(\left(\mathbf{D}_{ch,0} + \varepsilon \mathbf{D}_{ch,1} + O\left(\varepsilon^2\right)\right) \nabla \left(c_0 + \varepsilon c_1 + O\left(\varepsilon^2\right)\right)\right) \tag{4}$$

Notice $\mathbf{D}_{ch}$ may also fluctuate, since it is a function of c due to any non-ideal interaction between the ions and the host material. The expanded terms can be collected according to their orders in ε, to give a set of linear differential equations to be successively solved. When the system is perturbed around an uniform reference state, the zero-order problem is trivial and results in the gradient-free solution, where $\nabla c_0 = 0$. The ε-order problem, by which the impedance response is defined, can then be reduced to an ordinary linear differential equation in the frequency-space domain through Fourier transformation.

$$i\omega \hat{c} = \nabla \cdot (\mathbf{D}_{ch} \nabla \hat{c}) \tag{5}$$

Hereby we denote the chemical diffusivity tensor evaluated at the reference state simply by $\mathbf{D}_{ch}$, instead of $\mathbf{D}_{ch,0}$. Likewise, for any Fourier transformed equations in this article, parameters without the caret notation ($\hat{\square}$) represent their values evaluated at the reference state. Note that the $\mathbf{D}_{ch,1}$ term would survive in the ε-order problem, if the reference state has non-uniform composition. Given the linearity approximation is valid, the higher-order solutions are negligible compared to the ε-order solution, and Equation (5) governs the transport of charge carriers in the system.

Transport of charge carriers in active material has been described by current flow in a distributed RC transmission line [50,51]. Isotropic transport in traditional approach could be modeled using a 1D transmission line shown in Figure 1 (a). In the circuits, the grid in black corresponds to the ion pathways and its resistors represent drag that ions experience when they transport in the active material. The other grid in grey corresponds to the electron pathways, and it has negligible resistance between the nodes when electron mobility is high enough. Likewise, anisotropic transport can be modeled using a 2D or a 3D transmission line shown in Figure 1 (b) and (c), where the resistors between the nodes have different resistance values depending on the direction. The circuits may be connected to various terminating structures depending on the particle environment [17].

2.2. Anisotropic surface kinetics

To focus on the effects of anisotropic surface kinetics, we consider a simple interface model, where the active material is in direct contact with the electrolyte solution without any additional resistive layer, such as solid electrolyte interface (SEI) layer. On the

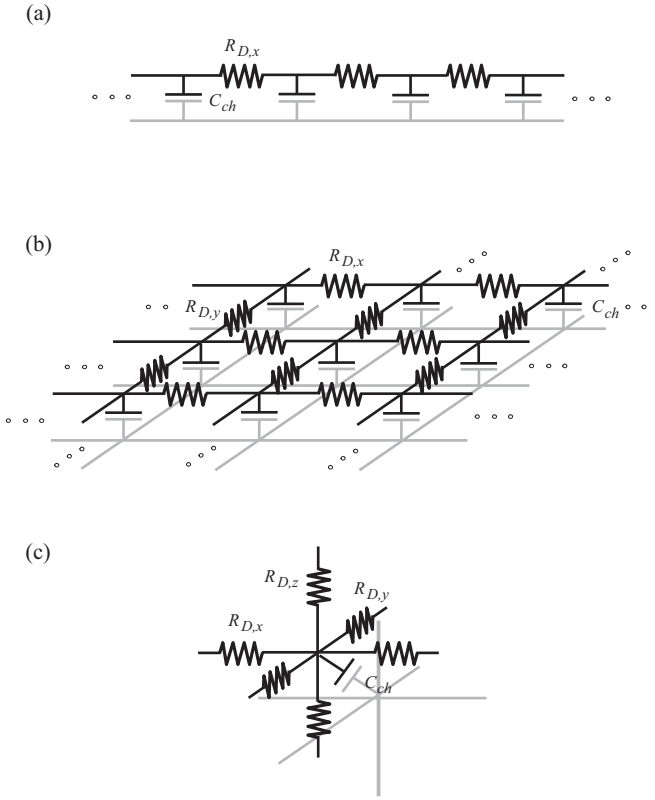

Fig. 1. Transmission line models describing transport of charge carriers in active material: (a) a 1D transmission line model, (b) a 2D transmission line model, and (c) a repeating node of a 3D transmission line model. $R_{D,x}$, $R_{D,y}$, and $R_{D,z}$ are the differential resistance of ion diffusion in the corresponding direction, and C_{ch} is the differential chemical capacitance [50,51].

electrolyte/active material interface, the ion insertion kinetics can be modeled by the Butler-Volmer equation. When the insertion rate is different according to the surface orientation with respect to the crystallographic axes, parameters in the equation should be functions of the surface orientation.

$$j_{ins} = j_0(\mathbf{n})\left[\exp\left(-\alpha(\mathbf{n})\frac{e\eta}{kT}\right) - \exp\left((1-\alpha(\mathbf{n}))\frac{e\eta}{kT}\right)\right] \tag{6}$$

where j_{ins} and $j_0(\mathbf{n})$ are the insertion current density and the exchange current density, respectively. e is the electron charge constant, $\mathbf{n}$ is the surface normal vector, $\alpha(\mathbf{n})$ is the transfer coefficient ($0 < \alpha < 1$), and $\eta = \Delta\phi - \Delta\phi_{eq}$ is the surface overpotential. Notice that j_0 and α are now functions of the surface normal vector, $\mathbf{n}$.

Applying the regular perturbation analysis to Equation (6), we can collect ε-order terms to calculate the impedance response for the insertion reaction. When the system is perturbed around an equilibrium reference state, fluctuations in j_0 and α do not effectively contribute to the impedance response, since the two exponential terms balance out each other. On the other hand, perturbation in $\Delta\phi_{eq}$ brings the contribution of surface ion concentration. Taking the Fourier transformation, perturbation in j_{ins} can be expressed by the following equation.

$$\hat{j}_{ins} = \frac{1}{\rho_{ct}(\mathbf{n})}\left(\Delta\hat{\phi} - \left(\frac{\partial\Delta\phi_{eq}}{\partial c}\right)\hat{c}_s\right) \tag{7}$$

where $\rho_{ct}(\mathbf{n}) = kT/(j_0(\mathbf{n})e)$ is the charge transfer resistance and $\partial\Delta\phi_{eq}/\partial c$ is the Nernst shift coefficient, both evaluated at the reference state. $\hat{c}_s$ is the surface ion concentration, which may have different values depending on the position. In more general, $\Delta\phi_{eq}$ as well as $\partial\Delta\phi_{eq}/\partial c$ may also depend on surface orientation, but we leave these subtle effects out of consideration and focus on $\rho_{ct}(\mathbf{n})$ only as a measure of anisotropy in surface kinetics.

The Faraday's law can be applied at the electrolyte/active material interface to correlates j_{ins} and the ion flux in the active material. The insertion current can then be represented as:

$$\hat{j}_{ins} = -e\left(\mathbf{D}_{ch}\left(\nabla\hat{c}\right)_s\right)\cdot\mathbf{n} \tag{8}$$

where $\left(\nabla\hat{c}\right)_s$ is the ion concentration gradient at the surface. When it is used together with the Butler-Volmer model in Equation (7), they present a boundary condition governing the ion transport in active material.

$$-e\left(\mathbf{D}_{ch}\left(\nabla\hat{c}\right)_s\right)\cdot\mathbf{n} = \frac{1}{\rho_{ct}(\mathbf{n})}\left(\Delta\hat{\phi} - \left(\frac{\partial\Delta\phi_{eq}}{\partial c}\right)\hat{c}_s\right) \tag{9}$$

With this boundary condition, the anisotropic diffusion equation, Equation (5), can be integrated twice to give the ion concentration field in the system. Here, we neglected surface diffusion of charge carriers, which can be important in other studies [52].

2.3. Anisotropic interface capacitance

Another electrochemical process taking place on the interface is accumulation of charge carriers, and it can be described by the ideal capacitor model. While capacitance from diffuse double layer should be fairly isotropic, pseudocapacitance, if there is any, should depend on surface orientation as it arises from surface-specific side reactions. To consider such anisotropy in surface accumulation, the capacitance should be given as a function of the surface orientation.

$$j_{acc} = C_{surf}(\mathbf{n})\frac{d\Delta\phi}{dt} \tag{10}$$

where j_{acc} is the accumulation current density on the interface, and $C_{surf}(\mathbf{n})$ is the surface capacitance. Applying the regular perturbation analysis and the Fourier transformation, Equation (10) can be mapped into the frequency domain for impedance calculation.

$$\hat{j}_{acc} = i\omega C_{surf}(\mathbf{n})\Delta\hat{\phi} \tag{11}$$

Other models for surface accumulation, including the constant phase element (CPE), can also be generalized to account for the anisotropy, in the similar manner.

2.4. Definitions of impedance functions

For each of the electrochemical processes, a local impedance function [53] can be defined on an infinitesimal area of active particle surface. To begin with diffusion impedance, contribution of the ion diffusion appears through the equilibrium potential of the insertion reaction, $\Delta\phi_{eq}$, due to the Nernst equilibrium correlation. Therefore, the local diffusion impedance is defined with the partial derivative of $\Delta\phi_{eq}$ with respect to c:

$$z_D = \frac{\Delta\hat{\phi}_{eq}}{\hat{j}_{ins}} = \left(\frac{\partial\Delta\phi_{eq}}{\partial c}\right)\frac{\hat{c}_s}{\hat{j}_{ins}} \tag{12}$$

where z_D is the local diffusion impedance. Employing this definition, Equation (7) can be rearranged into a generalized Ohm's form, which leads to the definition of local insertion impedance.

$$z_{ins} = \frac{\Delta\hat{\phi}}{\hat{j}_{ins}} = \rho_{ct}(\mathbf{n}) + z_D \tag{13}$$

where z_{ins} is the local insertion impedance. It implies a circuit analogy of the ion insertion process, a series circuit of ρ_{ct} and z_D, in a small perturbation regime. On the other hand, the impedance

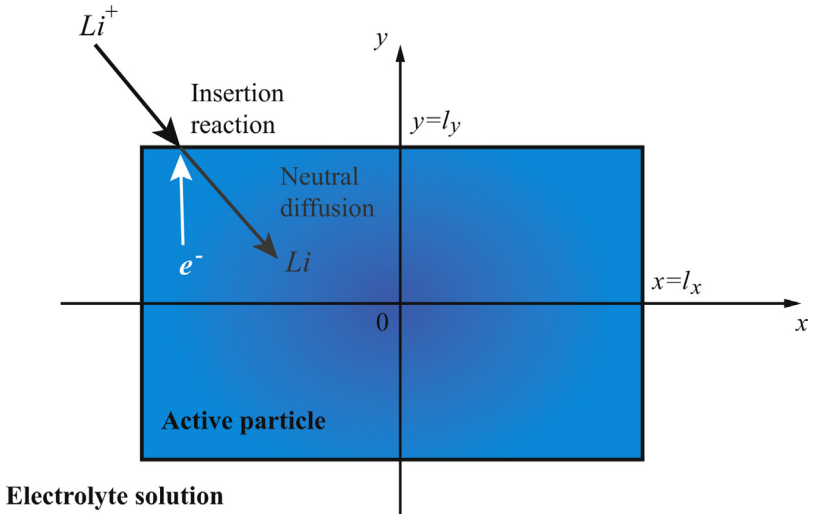

Fig. 2. Anisotropic 2D rectangular particle in electrolyte solution, and behavior of charge carriers in the system.

function corresponding to the charge carrier accumulation on the surface can be defined independently from Equation (11).

$$z_{acc} = \frac{\Delta\hat{\phi}}{\hat{j}_{acc}} = \frac{1}{i\omega C_{surf}(\mathbf{n})} \tag{14}$$

where z_{acc} is the local accumulation impedance.

The total local impedance is the combined response of these, and it is related to the activeness of a specific position on particle surface. We assume independent parallel contributions of j_{ins} and j_{acc} on particle surface, following Randles [14].

$$\hat{j}_{tot} = \hat{j}_{ins} + \hat{j}_{acc} \tag{15}$$

where j_{tot} is the total current density. The total local impedance then can be defined using j_{tot}.

$$z_{tot} = \frac{\Delta\hat{\phi}}{\hat{j}_{tot}} = \frac{\Delta\hat{\phi}}{\hat{j}_{ins}+\hat{j}_{acc}} = \left(z_{ins}^{-1}+z_{acc}^{-1}\right)^{-1} = \left((\rho_{ct}(\mathbf{n})+z_D)^{-1}+z_{acc}^{-1}\right)^{-1} \tag{16}$$

where z_{tot} is the total local impedance. As implied by the expression, z_{tot} can be represented by the Randles equivalent circuit, which has C_{surf} in parallel with a series of ρ_{ct} and z_D.

The particle impedance is defined by a collective response of local impedance on the entire surface of a particle. Its definition therefore employs the total current on the particle surface, which can be obtained by integrating j_{tot} over the particle surface area. The potential is assumed homogeneous on the entire particle surface due to high electron mobility. Then, the particle impedance can be defined as:

$$Z_p = \frac{\Delta\hat{\phi}}{\hat{J}_p} = \frac{\Delta\hat{\phi}}{\int_{A_p}\hat{j}_{tot}dS} = \left(\int_{A_p} z_{tot}^{-1}dS\right)^{-1} \tag{17}$$

where Z_p is the particle impedance, J_p is the total current on the particle surface, and A_p is the particle surface area. Z_p can be considered as a harmonic average of z_{tot} over the particle surface. In terms of equivalent circuit, local impedance elements are arranged in parallel or side by side to constitute Z_p.

Expanding our view to the overall electrode, the overall electrode impedance is a collective response of all particles in an electrode. Thus, its definition employs the overall current summed over the particle population. When there are distributions in particle properties, it is useful to convert the summation to an integral over the distributions. It can be done by defining continuous random variables that represent the distributed particle properties.

$$Z_{ov} = \frac{\Delta\hat{\phi}}{\hat{J}_{ov}} = \frac{\Delta\hat{\phi}}{\sum_{n_p=1}^{N_p}\hat{J}_{p,n_p}} = \frac{\Delta\hat{\phi}}{N_p\int_\Omega Pr_{\mathbf{v}_d}(\mathbf{v}_d)\hat{J}_p(\mathbf{v}_d)\,d\mathbf{v}_d} = N_p^{-1}\left(\int_\Omega Pr_{\mathbf{v}_d}(\mathbf{v}_d)Z_p^{-1}(\mathbf{v}_d)\,d\mathbf{v}_d\right)^{-1} \tag{18}$$

where Z_{ov} is the overall electrode impedance, $\hat{J}_{ov}$ is the overall electrode current, n_p and N_p are the numbering index and the number of active particles in the electrode, respectively. When Z_{ov} is defined with the integral over distributed particle parameters, $\mathbf{v}_d$ is a realization of the random variable vector, $\mathbf{VSSS}_d$, where each component represents one of the distributed parameters. $Pr_{\mathbf{v}_d}$ is then the joint probability density function (PDF) of $\mathbf{V}_d$, and $\boldsymbol{\Omega}$ is the domain in which $\mathbf{V}_d$ is defined. $\mathbf{V}_d$ may have diffusivities, resistances, and lengths in different directions for its components. Arriving at Equation (18), we assumed that the ion conductivity in the electrolyte solution is high and/or the electrode is thin enough, so that any gradient along the electrode thickness was not considered. Otherwise, the impedance definitions presented here can be incorporated into the impedance models of thick porous electrodes suggested in References [17] and [23].

3. Impedance of an Anisotropic 2D Rectangular Particle

In this section, we focus on the impedance behavior of an anisotropic 2D rectangular particle shown in Figure 2. It can be considered as a hypothetic 2D particle or a rectangular cross-section of a rod-shaped particle, which is fully submerged in the electrolyte solution with small contacts to conductive materials. With this system, we can fully study the effects of anisotropies on the impedance behavior with minimal complexity. To obtain the impedance behavior, we need to solve the ion transport problem, which is reduced to a 2D boundary value partial differential equation (PDE) problem. The governing diffusion equation is:

$$i\omega\hat{c} = D_{ch,x}\frac{\partial^2\hat{c}}{\partial x^2} + D_{ch,y}\frac{\partial^2\hat{c}}{\partial y^2} \tag{19}$$

The boundary conditions come from the Butler-Volmer model and the system symmetry.

$$\begin{aligned} -eD_{ch,x}\left.\frac{\partial \hat{c}}{\partial x}\right|_{x=l_x} &= \frac{1}{\rho_{ct,x}}\left(\Delta\hat{\phi} - \left(\frac{\partial \Delta\phi_{eq}}{\partial c}\right)\hat{c}\big|_{x=l_x}\right) \\ -eD_{ch,y}\left.\frac{\partial \hat{c}}{\partial y}\right|_{y=l_y} &= \frac{1}{\rho_{ct,y}}\left(\Delta\hat{\phi} - \left(\frac{\partial \Delta\phi_{eq}}{\partial c}\right)\hat{c}\big|_{y=l_y}\right) \\ \left.\frac{\partial \hat{c}}{\partial x}\right|_{x=0} &= 0 \\ \left.\frac{\partial \hat{c}}{\partial y}\right|_{y=0} &= 0 \end{aligned} \tag{20}$$

where $\rho_{ct,x} = \rho_{ct}(\mathbf{e}_x)$ and $\rho_{ct,y} = \rho_{ct}(\mathbf{e}_y)$ are the charge transfer resistances on x and y normal surfaces, respectively. l_x and l_y are the one halves of the particle lengths in corresponding directions, as shown in Figure 2.

The variables in Equations (19) and (20) can be nondimensionalized using appropriate scales. The dimensionless concentration can be defined by $\hat{\tilde{c}} = \left(-\partial\Delta\phi_{eq}/\partial c\right)\hat{c}/\Delta\hat{\phi}$, and the dimensionless spatial variables by $\tilde{x} = x/l_x$ and $\tilde{y} = y/l_y$. Further scaling becomes simpler when we define frequency scales and resistance scales for diffusion in each direction: $\omega_{D,x} = D_{ch,x}/l_x^2$, $\omega_{D,y} = D_{ch,y}/l_y^2$, $\rho_{D,x} = \left(-\partial\Delta\phi_{eq}/\partial c\right) l_x/eD_{ch,x}$, and $\rho_{D,y} = \left(-\partial\Delta\phi_{eq}/\partial c\right) l_y/eD_{ch,y}$, where $\omega_{D,x}$ and $\omega_{D,y}$ are the diffusion characteristic frequencies in x and y directions, and $\rho_{D,x}$ and $\rho_{D,y}$ are the diffusion characteristic resistances in x and y directions, respectively. Then, it turns out that four dimensionless numbers govern the ion transport in the system. Two are ratios of the frequency scales: $\tilde{\omega} = \omega/\omega_{D,x}$ and $\tau = \omega_{D,y}/\omega_{D,x}$. The other two are ratios of the diffusion characteristic resistance and the charge transfer resistance on each surface: $\beta_x = \rho_{D,x}/\rho_{ct,x}$ and $\beta_y = \rho_{D,y}/\rho_{ct,y}$. Each of the resistance ratios indicates relative insertion rate on the surfaces and diffusionrate in the bulk system, like a Biot number in traditional transport systems involving boundary fluxes. Employing the dimensionless variables and the scaled parameters, the governing equation and the boundary conditions become

$$\begin{aligned} i\tilde{\omega}\hat{\tilde{c}} &= \frac{\partial^2\hat{\tilde{c}}}{\partial\tilde{x}^2} + \tau\frac{\partial^2\hat{\tilde{c}}}{\partial\tilde{y}^2} \\ -\beta_x^{-1}\left.\frac{\partial\hat{\tilde{c}}}{\partial\tilde{x}}\right|_{\tilde{x}=1} &= 1 + \hat{\tilde{c}}\big|_{\tilde{x}=1} \\ -\beta_y^{-1}\left.\frac{\partial\hat{\tilde{c}}}{\partial\tilde{y}}\right|_{\tilde{y}=1} &= 1 + \hat{\tilde{c}}\big|_{\tilde{y}=1} \\ \left.\frac{\partial\hat{\tilde{c}}}{\partial\tilde{x}}\right|_{\tilde{x}=0} &= 0 \\ \left.\frac{\partial\hat{\tilde{c}}}{\partial\tilde{y}}\right|_{\tilde{y}=0} &= 0 \end{aligned} \tag{21}$$

Such a boundary value PDE problem, defined in a finite domain, can be solved analytically by the finite Fourier transformation (FFT) method [54]. Mathematical works involved in deriving the solution are presented in Appendix B. The solution for $\hat{\tilde{c}}$ is given by

$$\hat{\tilde{c}}(\tilde{x},\tilde{y}) = -1 + \sum_{k=1}^{\infty}\Gamma_k\left(1 - \frac{\beta_y\cosh(\Lambda_k\tilde{y})}{\beta_y\cosh(\Lambda_k) + \Lambda_k\sinh(\Lambda_k)}\right)B_k\cos(\lambda_k\tilde{x}) \tag{22}$$

where λ_k, B_k, Λ_k, and Γ_k are defined in Appendix B.

The particle impedance includes parallel contributions from the charge accumulation and the ion insertion. Under such an arrangement, a resistive-capacitive (RC) characteristic frequency naturally arises for each of x normal and y normal surfaces: $\omega_{RC,x} = \left(\rho_{ct,x}C_{surf,x}\right)^{-1}$ and $\omega_{RC,y} = \left(\rho_{ct,y}C_{surf,y}\right)^{-1}$, where $C_{surf,x} = C_{surf}(\mathbf{e}_x)$ and $C_{surf,y} = C_{surf}(\mathbf{e}_y)$. While various scaling strategies could be employed depending on the characteristics to be studied, the local impedance functions are scaled by $\rho_{ct,x}$, and Z_p is scaled by $\left(\rho_{ct,x}/8l_y\right)$ in this article. Using the definition in Equation (17), the dimensionless particle impedance becomes

$$\begin{aligned} \tilde{Z}_p &= \left(\frac{8l_y}{\rho_{ct,x}}\right)Z_p \\ &= \left(\frac{1}{2}\int_0^1\left(\tilde{z}_{tot}\big|_{\tilde{x}=1}\right)^{-1}d\tilde{y} + \frac{1}{2}\gamma\int_0^1\left(\tilde{z}_{tot}\big|_{\tilde{y}=1}\right)^{-1}d\tilde{x}\right)^{-1} \end{aligned} \tag{23}$$

where $\tilde{z}_{tot} = z_{tot}/\rho_{ct,x}$ is the dimensionless local total impedance, and $\gamma = l_x/l_y$ is the geometric aspect ratio of the particle. Expanding $\tilde{z}_{tot}$ according to Equation (16) and performing the integrals, an analytical expression for $\tilde{Z}_p$ is obtained. Detailed algebraic and calculus steps are given in Appendix C.

$$\begin{aligned} \tilde{Z}_p^{-1} &= \left(\frac{i\tilde{\omega}}{2}\right)\left(\frac{1}{\chi_x} + \frac{\gamma}{\nu\tau\chi_y}\right) \\ &+ \frac{1}{2}\sum_{k=1}^{\infty}\Gamma_k B_k\left(\cos(\lambda_k) + \frac{\left(\frac{\gamma\Lambda_k}{\nu\lambda_k}\right)\sinh(\Lambda_k)\sin(\lambda_k) - \beta_y sinh(\Lambda_k)\cos(\lambda_k)}{\Lambda_k\beta_y\cosh(\Lambda_k) + \Lambda_k^2\sinh(\Lambda_k)}\right) \end{aligned} \tag{24}$$

where $\nu = \rho_{ct,y}/\rho_{ct,x}$, $\chi_x = \omega_{RC,x}/\omega_{D,x}$, $\chi_y = \omega_{RC,y}/\omega_{D,y}$, and $\gamma = l_x/l_y$ are additionally identified as dimensionless numbers governing the system response. Therefore, in total, eight dimensionless numbers are found to determine the behavior of the particle impedance. Table 1 shows values of the parameters, the characteristic scales, and the dimensionless numbers for the isotropic reference case [17,23]. In examining $\tilde{Z}_p$ under various anisotropies, the corresponding parameters are varied for a certain range.

Table 1
Isotropic reference values of parameters, characteristic scales and dimensionless numbers [23].

Property	Value	Unit
$\left(-\partial\Delta\phi_{eq}/\partial c\right)$	20.27	Vcm^3/mol
$D_{ch,x}$, $D_{ch,y}$	1.0×10^{-9}	cm^2/s
$\rho_{ct,x}$, $\rho_{ct,y}$	44.06	Ωcm^2
$C_{surf,x}$, $C_{surf,y}$	1.0×10^{-5}	F/cm^2
l_x, l_y	2.0×10^{-4}	cm
$\rho_{D,x}$, $\rho_{D,y}$	46.16	Ωcm^2
$\omega_{D,x}$, $\omega_{D,y}$	2.5×10^{-2}	s^{-1}
$\omega_{RC,x}$, $\omega_{RC,y}$	2.3×10^{3}	s^{-1}
β_x, β_y	1.05	–
χ_x, χ_y	9.08×10^{4}	–
ν	1	–
τ	1	–
γ	1	–

3.1. Effects of Anisotropic Diffusion

The effect of anisotropic diffusion can be examined by using the $\tilde{Z}_p$ solution in Equation (24) and the parameters in Table 1, and varying one of the diffusivity values. Figure 3 shows behavior of $\tilde{Z}_p$ under various extents of anisotropy in diffusion. $D_{ch,y}$ is gradually changed by $D_{ch,y} = 10^{\kappa}D_{ch,x}$ for $\kappa = -2, -1, 0, 1, 2$, while $D_{ch,x}$ is fixed at the reference value. As described in the complex plane plot, Figure 3 (a), various slopes can be obtained in the Warburg regime when the diffusion becomes anisotropic. While the slope is around 45° for the isotropic reference case, it becomes lower when diffusion in one direction is slower, and it becomes higher when

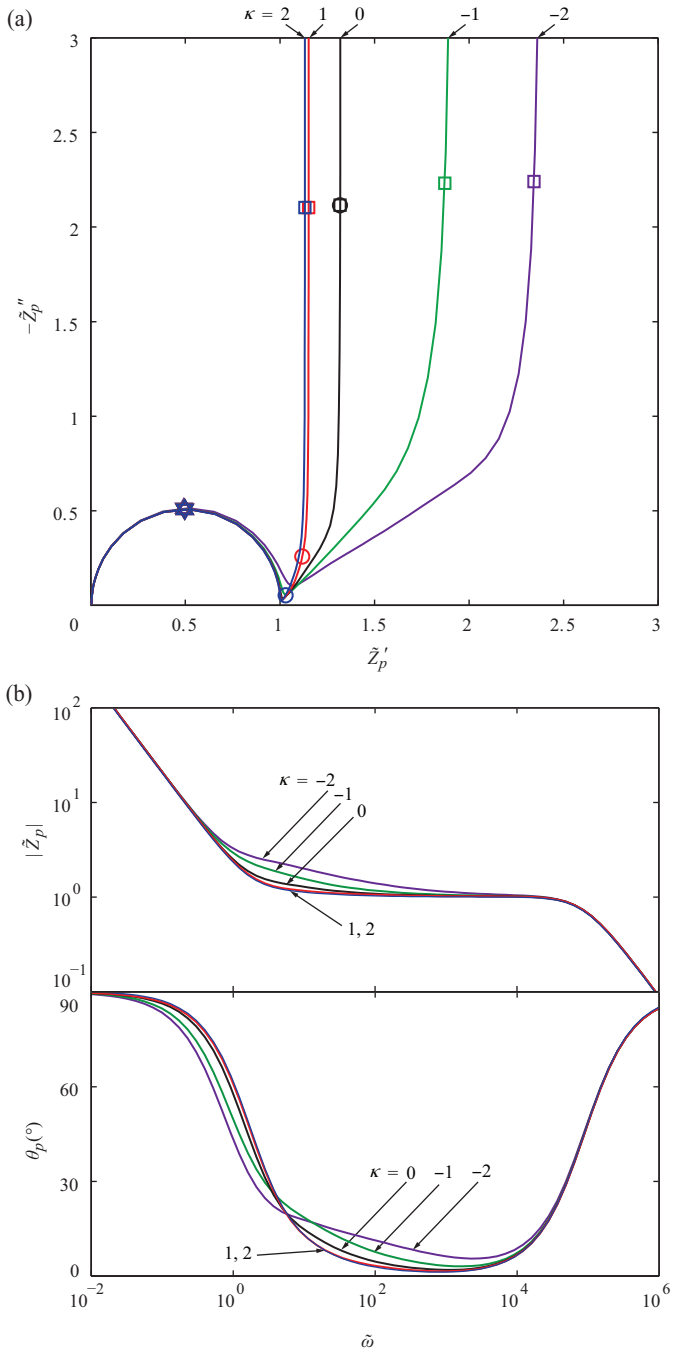

Fig. 3. Particle impedance varying the extent of anisotropy in diffusion: (a) a complex plane plot, (b) magnitude and phase angle plots, which are also called a Nyquist plot and Bode plots, respectively. $D_{ch,y}$ is changed by $D_{ch,y} = 10^{\kappa} D_{ch,x}$ for $\kappa = -2, -1, 0, 1, 2$, while $D_{ch,x}$ is fixed at 1.0×10^{-9}cm^2/s. For each curve, △, ▽, □, and ○ represent $\tilde{Z}_p$ at $\tilde{\omega} = \chi_x$, χ_y, 1, and, τ, respectively.

diffusion in one direction is faster. In the magnitude and the phase angle plots, Figure 3 (b), transitions still take place near $\tilde{\omega} \approx 1$ and $\tilde{\omega} \approx 10^5$ with little change in its shape or magnitude.

When the charge transfer resistance and the diffusion characteristic resistance are comparable in one of the directions, like in the above case where $\beta_x \approx 1$, the ion transport is strongly aligned with the direction in the Warburg regime. Therefore in Figure 3, it is the diffusion in x direction that determines the transition and the magnitude of the diffusion impedance. The transition thus remains near $\tilde{\omega} \approx 1$, equivalently $\omega \approx \omega_{D,x}$, and the Warburg regime keeps its magnitude around $\rho_{D,x}$, even though $\rho_{D,y}$ varies by orders. On the other hand, a significant amount of ions still pass through the y normal surfaces since the charge transfer resistances at both x normal and y normal surfaces are the same. There is local accumulation of ions near y normal surfaces when the diffusion in y direction becomes slower, and ions tend to be quickly distributed homogeneously along the direction when the diffusion becomes faster. The local accumulation gives the resistive contribution, and the homogenous distribution gives the capacitive contribution to the Warburg regime, varying its slope.

In particular, when $D_{ch,y} \gg D_{ch,x}$ in the above case with $\beta_x \approx 1$ and $\nu \approx 1$, the Gerischer limit can be defined. In more general, the Gerischer limit can be found when the system has strong anisotropy in diffusion but has relatively even insertion rate. Additionally, the largest diffusion characteristic resistance and the charge transfer resistances should be similar in order. Under such conditions, the ion flux through the surface normal to the faster diffusion direction could be analogized by a homogenous reaction that simultaneously taking place with 1D diffusion in the slower direction. Therefore, in the Gerischer limit, the combined response of the 2D diffusion and the surface insertion can be approximated by the 1D Gerischer impedance, by averaging the variables over the cross-section normal to the slower diffusion direction. Then, the transport problem is reduced to a typical 1D diffusion-reaction problem, and its response can be obtained in an analytical form:

$$\tilde{Z}_{p,G}^{-1} = \left(\frac{i\tilde{\omega}}{2}\right)\left(\frac{1}{\chi_x} + \frac{\gamma}{\nu\tau\chi_y}\right) + \frac{1}{2}\left[\left(1 + \frac{\tau\beta_y}{i\tilde{\omega}}\right)\left(1 + \frac{\beta_x \coth(\zeta)}{\zeta}\right)\right]^{-1} \quad (25)$$

where $\tilde{Z}_{p,G}$ is the Gerischer limit of particle impedance, and $\zeta = \sqrt{i\tilde{\omega} + \tau\beta_y}$. As implied by its name, a bounded Gerischer impedance function, $\beta_x \coth(\zeta)/\zeta$, can be found in place of the diffusion impedance. Detailed derivation of the solution is shown in Appendix D.

Such trends, however, are not general but depend on the parameter values and the corresponding dimensionless numbers. For instance, if $\beta_x \gg 1$ and $\beta_y \gg 1$, the insertion reaction stays near its equilibrium, and the ions are supplied at the surface as quickly as they diffuse away. Therefore, the system response is largely determined by the ion diffusion, and the charge transfer resistance appears negligible compared to the diffusion impedance. When the diffusion becomes strongly anisotropic, either $D_{ch,x} \gg D_{ch,y}$ or $D_{ch,x} \ll D_{ch,y}$, the response approaches that of 1D diffusion. The magnitude and the transition frequency of the diffusion impedance are then solely determined by the diffusion in the faster direction. On the other hand, when $\beta_x \ll 1$ and $\beta_y \ll 1$, the ions diffuse quickly throughout the system as soon as inserted, and it is the ion insertion rate that determines the system response. In this case, contribution of the ion diffusion appears as a purely capacitive behavior at frequencies lower than the RC characteristic frequencies, and the anisotropy in diffusion does not affect the impedance behavior.

3.2. Effects of Anisotropic Surface Kinetics

The effect of anisotropic surface kinetics can be examined by varying one of the charge transfer resistance values. Figure 4 shows behavior of $\tilde{Z}_p$ under various extents of anisotropy in surface kinetics, using the parameter values in Table 1. Among the parameters, $\rho_{ct,y}$ is gradually changed by $\rho_{ct,y} = 10^{\kappa}\rho_{ct,x}$ for $\kappa = -2, -1, 0, 1, 2$, while $\rho_{ct,x}$ is fixed at the reference value. The change in $\tilde{Z}_p$ is

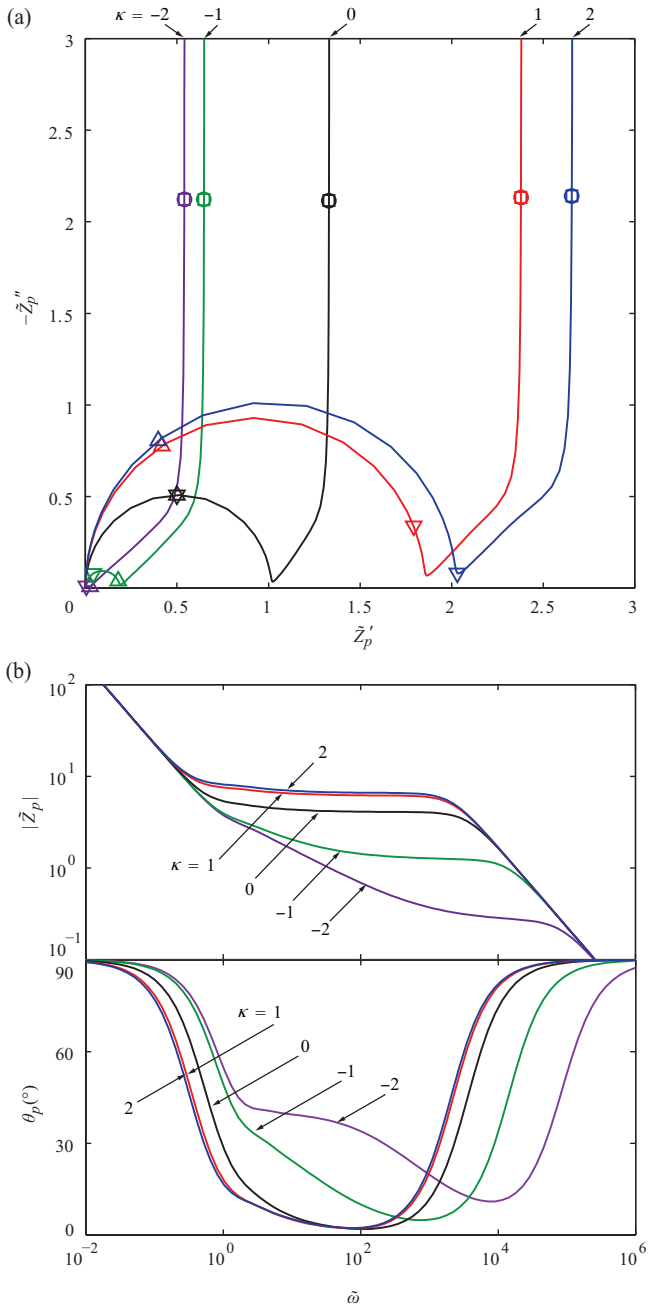

Fig. 4. Particle impedance varying the extent of anisotropy in surface kinetics: (a) a complex plane plot, (b) magnitude and phase angle plots. $\rho_{ct,y}$ is changed by $\rho_{ct,y} = 10^{\kappa}\rho_{ct,x}$ for $\kappa = -2, -1, 0, 1, 2$, while $\rho_{ct,x}$ is fixed at 44.06 Ωcm^2. For each curve, △, ▽, □, and ○ represent $\tilde{Z}_p$ at $\tilde{\omega} = \chi_x$, χ_y, 1, and, τ, respectively.

better explained by defining the particle surface resistance and the particle surface capacitance.

$$R_p = \left(\frac{4l_y}{\rho_{ct,x}} + \frac{4l_x}{\rho_{\mathrm{ct,y}}}\right)^{-1} \tag{26}$$

$$C_p = 4l_y C_{surf,x} + 4l_x C_{surf,y} \tag{27}$$

where R_p and C_p are the particle surface resistance and capacitance, respectively. The corresponding dimensionless parameters are $\tilde{R}_p = 8l_y R_p/\rho_{ct,x}$ and $\tilde{C}_p = \omega_{D,x}\rho_{ct,x}C_p/8l_y$. In Figure 4 (a), the diameter of the RC semicircle represents $\tilde{R}_p$. When $\rho_{ct,y}$ decreases, the diameter shrinks together, but it converges to 2 when $\rho_{ct,y}$ increases. At this limit, as y normal surfaces are being blocked, most ions intercalate through x normal surfaces, and $\tilde{R}_p$ is determined by $\rho_{ct,x}$. The RC characteristic frequency of the particle impedance is defined by $\tilde{\omega}_{RC,p} = \left(\tilde{R}_p\tilde{C}_p\right)^{-1}$. In Figure 4 (b), the RC transition takes place at higher frequencies when $\rho_{ct,y}$ decrease, but when $\rho_{ct,y}$ increases, the transition frequency does not change significantly.

There is one more interesting aspect in this result: the anisotropy in surface kinetics also affects the diffusion impedance. Whenever $\rho_{ct,y}$ decreases or increases, if the two charge transfer resistances differ significantly, the diffusion impedance approaches its 1D limit. As shown in the complex plane plot, Figure 4 (a), the Warburg regime becomes straighter and less steep for both $\kappa = -2$ and $\kappa = 2$. In such conditions, the majority of ions intercalate through the less resistive surfaces, and their diffusion becomes effectively one dimensional, normal to the surface. For example, when $\rho_{ct,y} \gg \rho_{ct,x}$, the majority of ions intercalate through x normal surfaces and diffuse predominantly in x direction. The diffusion impedance approaches its 1D limit that corresponds to the ion diffusion in x direction.

3.3. Effects of Anisotropic Surface Capacitance

Likewise, employing the solution of $\tilde{Z}_p$ and varying one of the surface capacitances, we can study the effect of anisotropy in surface capacitance. Figure 5 shows behavior of $\tilde{Z}_p$ under various extent of anisotropy in surface capacitance. $C_{surf,y}$ is gradually changed by $C_{surf,y} = 10^{\kappa}C_{surf,x}$ for $\kappa = -2, -1, 0, 1, 2$, while $C_{surf,x}$ is fixed at the reference value. As shown in Figure 5 (b), when $C_{surf,y}$ increases, the RC transition frequency, $\tilde{\omega}_{RC,p}$, shifts to a lower value. Accordingly in Figure 5 (a), the RC semicircle tends to be more convoluted with the diffusion impedance. On the other hand, the transition frequency changes by little when $C_{surf,y}$ decreases. The particle surface capacitance, $\tilde{C}_p$ in Equation (27), increases together with $C_{surf,y}$ when $C_{surf,y}$ increases, but it converges to the constant $C_{surf,x}$ when $C_{surf,y}$ shrinks. Therefore, $\tilde{\omega}_{RC,p}$, which is inversely proportional to $\tilde{C}_p$, shifts to a lower value when $C_{surf,y}$ increases, but it stays around the reference value when $C_{surf,y}$ decreases.

4. Overall Impedance of an Electrode with Anisotropic 2D Rectangular Particles

Now, we expand our view to the overall impedance of a battery electrode. The overall electrode impedance is a collective response of all the particles in an electrode, and is affected by distribution in the anisotropic properties among the particles. Consider a porous battery electrode that has hypothetic 2D rectangular particles or rod-shaped particles with rectangular cross-sections, as shown in Figure 6. In either case, impedance response of each particle can be described by $\tilde{Z}_p$ in Equation (24). For such electrodes, two of the apparent distributions are the length distributions of the particles or the cross-sections. Considering the two lengths as the distributed parameters of our concern, the overall electrode impedance in Equation (18) becomes:

$$\begin{aligned}\tilde{Z}_{ov} &= \left(\frac{8\bar{L}_y N_p}{\rho_{ct,x}}\right) Z_{ov} \\ &= \left(\int_0^{\infty}\int_0^{\infty} Pr_{\tilde{L}_x,\tilde{L}_y}\left(\tilde{l}_x,\tilde{l}_y\right)\tilde{Z}_p^{-1}\left(\tilde{l}_x,\tilde{l}_y\right)\tilde{l}_y d\tilde{l}_x d\tilde{l}_y\right)^{-1}\end{aligned} \tag{28}$$

where $\tilde{Z}_{ov}$ is the dimensionless overall electrode impedance. L_x and L_y are the random variables representing the length distributions in x and y directions, respectively, and $\tilde{L}_x = L_x/\bar{L}_x$ and $\tilde{L}_y = L_y/\bar{L}_y$ are the corresponding dimensionless random variables, scaled by their respective means, $\bar{L}_x$ and $\bar{L}_y$. Then, $\tilde{l}_x$ and $\tilde{l}_y$ are realizations of $\tilde{L}_x$ and $\tilde{L}_y$, respectively, and $Pr_{\tilde{L}_x,\tilde{L}_y}$ is the joint PDF of $\tilde{L}_x$ and $\tilde{L}_y$.

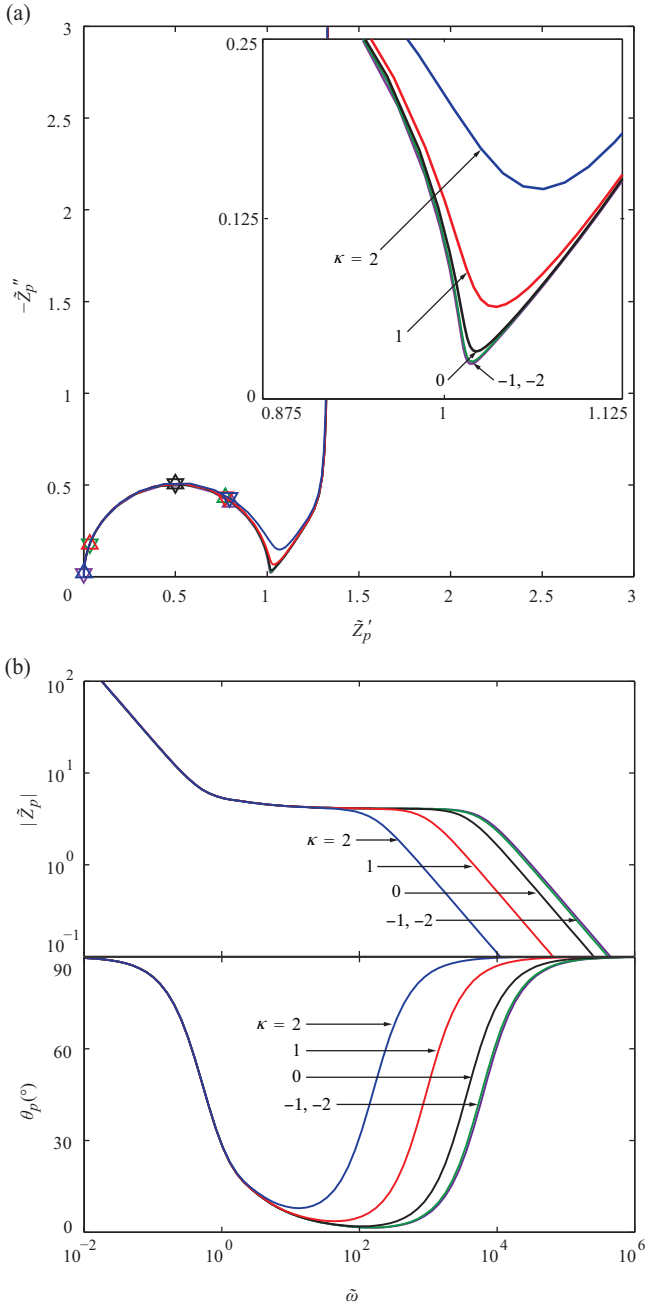

Fig. 5. Particle impedance varying the extent of anisotropy in surface capacitance: (a) a complex plane plot, (b) magnitude and phase angle plots. $C_{surf,x}$ is changed by $C_{surf,x} = 10^{\kappa} C_{surf,y}$ for $\kappa = -2, -1, 0, 1, 2$, while $C_{surf,y}$ is fixed at 1.0×10^{-5} F/cm^2. For each curve, △, ▽, □, and ○ represent $\tilde{Z}_p$ at $\tilde{\omega} = \chi_x$, χ_y, 1, and, τ, respectively.

$\tilde{Z}_p\left(\tilde{l}_x, \tilde{l}_y\right)$ is the dimensionless particle impedance we studied in the previous section, which is funtionalized in terms of $\tilde{l}_x$ and $\tilde{l}_y$. We employed a bivariate log-normal PDF to describe the distribution in $\tilde{L}_x$ and $\tilde{L}_y$. When parameters vary among the particles, the characteristic scales and the dimensionless numbers are redefined for the electrode using their mean values.

4.1. Effect of uncorrelated length distributions

Suppose the particles are strongly anisotropic, having faster diffusion in x direction and faster insertion kinetics on x normal surface. We set $D_{ch,x} = 20D_{ch,y}$ and $\rho_{ct,x} = 1/40\rho_{ct,y}$, while taking

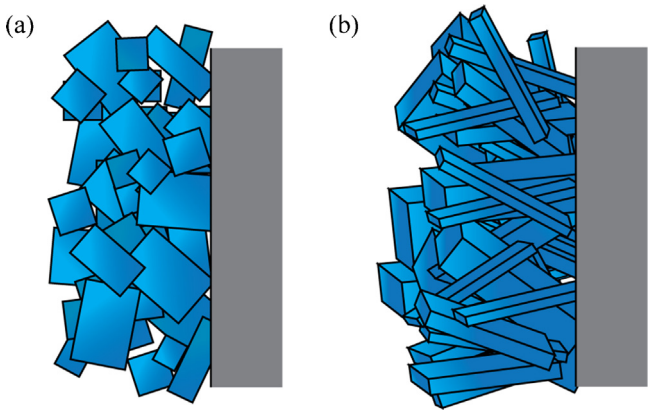

Fig. 6. Electrode configurations considered in Section 4: (a) an electrode with hypothetic 2D rectangular particles, and (b) an electrode with rod-like particles of rectangular cross-sections.

the reference values in Table 1 for $D_{ch,y}$, $\rho_{ct,y}$, and other parameters. In each particle, the agiler surface kinetics on x normal surface and the faster diffusion in x direction makes the majority of ions intercalate through x normal surface and diffuse mainly in x direction. Hence, the ion transport can be approximated by 1D transport in x direction. $\tilde{l}_x$ becomes the main diffusion length and $\tilde{l}_y$ becomes the secondary diffusion length. In the particle impedance, $\tilde{R}_p$ converges to 2, and the diffusion element approaches its 1D limit, corresponding to the diffusion in x direction, having the magnitude and the characteristic frequency of β_x and 1, respectively.

The random variables representing the length distributions, $\tilde{L}_x$ and $\tilde{L}_y$, may have various distributions. Figure 7 (a) shows scattered plots of their distributions employed in calculating $\tilde{Z}_{ov}$, where Σ_{xx}, Σ_{yy}, $\Sigma_{xy} = \Sigma_{yx}$ are the variance of $\tilde{L}_x$, the variance of $\tilde{L}_y$ and the covariance of $\tilde{L}_x$ and $\tilde{L}_y$. Each distribution is a bivariate log-normal distribution, and $\tilde{L}_x$ and $\tilde{L}_y$ are considered independent from each other at this time $\left(\Sigma_{xy} = \Sigma_{yx} = 0\right)$. Figure 7 (b) shows the complex plane plot of $\tilde{Z}_{ov}$ examined using the length distributions in Figure 7 (a). Only the distribution in main diffusion length, $\tilde{L}_x$, affects the impedance behavior, while the distribution in secondary diffusion length, $\tilde{L}_y$, has little effect. As $\tilde{L}_x$ spreads broader with increasing Σ_{xx}, the transition in diffusion impedance becomes smoother. Simultaneously, the capacitive regime starts deviating from the vertical behavior and shows a CPE-like behavior. Such trend is not affected by the change in Σ_{yy}, as long as the length distributions are independent. This is because ion intercalation and diffusion in each particle is nearly one-dimensional in x direction. The distribution in $\tilde{L}_x$ leads to dispersion in the transition frequency of diffusion impedance and makes the transition spread over a wide frequency range. This is similar to the effect of size distribution of isotropic particles in a battery electrode [16], as well as the effect of pore size distribution in a porous capacitor electrode [55,56].

4.2. Effect of correlated length distributions

It becomes a different story when the length distributions are correlated. Now we need to consider the fact that, in the rectangular geometry of the particles or the cross-sections, the secondary diffusion length, $\tilde{l}_y$, determines the effective surface area, or length, over which the majority of ions are being inserted. Thus, $\tilde{l}_y$ can also be defined as the main insertion area, which gives weighting on the transport response in the main diffusion direction. Figure 8 (a) shows scattered plots of correlated distributions with various ρ_{xy}, and constant Σ_{xx} and Σ_{yy}. As the distributions are more correlated with a larger ρ_{xy}, it becomes relatively more probable that large $\tilde{l}_x$

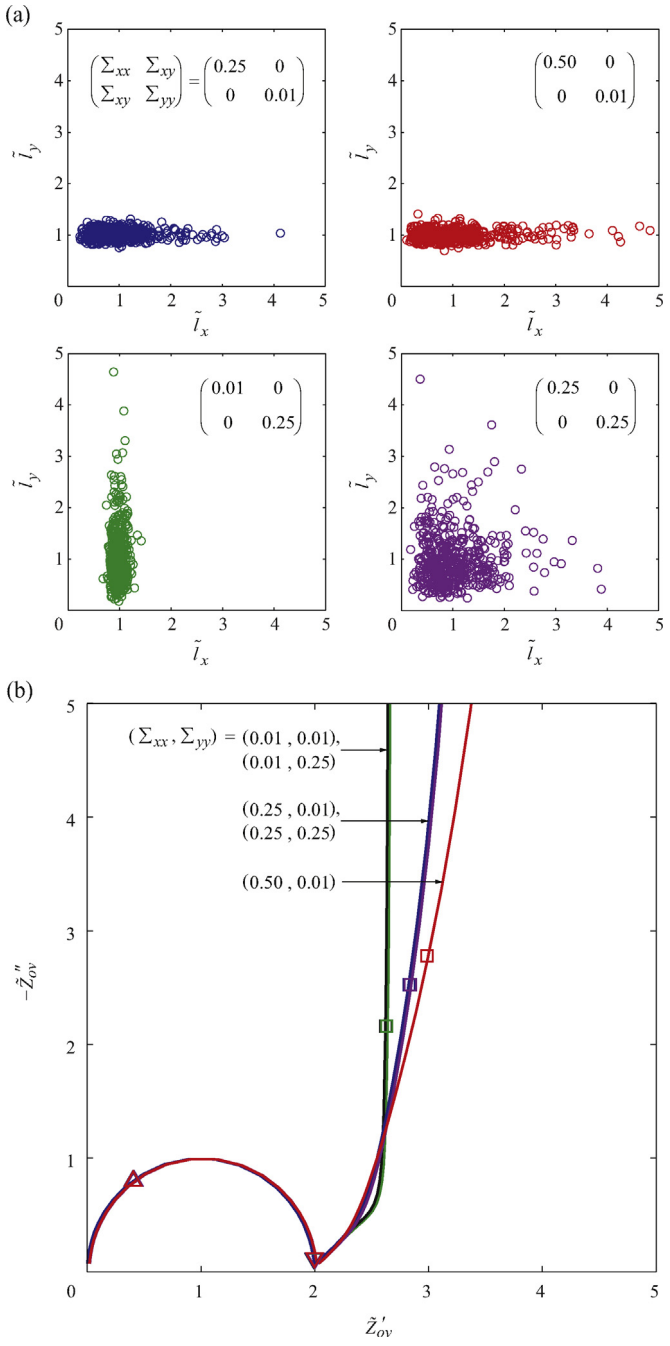

Fig. 7. (a) Uncorrelated length distributions with various covariance matrices, and (b) a complex plane plot of overall electrode impedance with the length distributions in (a). For each curve, △, ▽, and □ represent $\tilde{Z}_{ov}$ at $\tilde{\omega} = \chi_x$, χ_y, and 1, respectively. $\tilde{Z}_{ov}$ at $\tilde{\omega} = \tau$ raises out of the plot range.

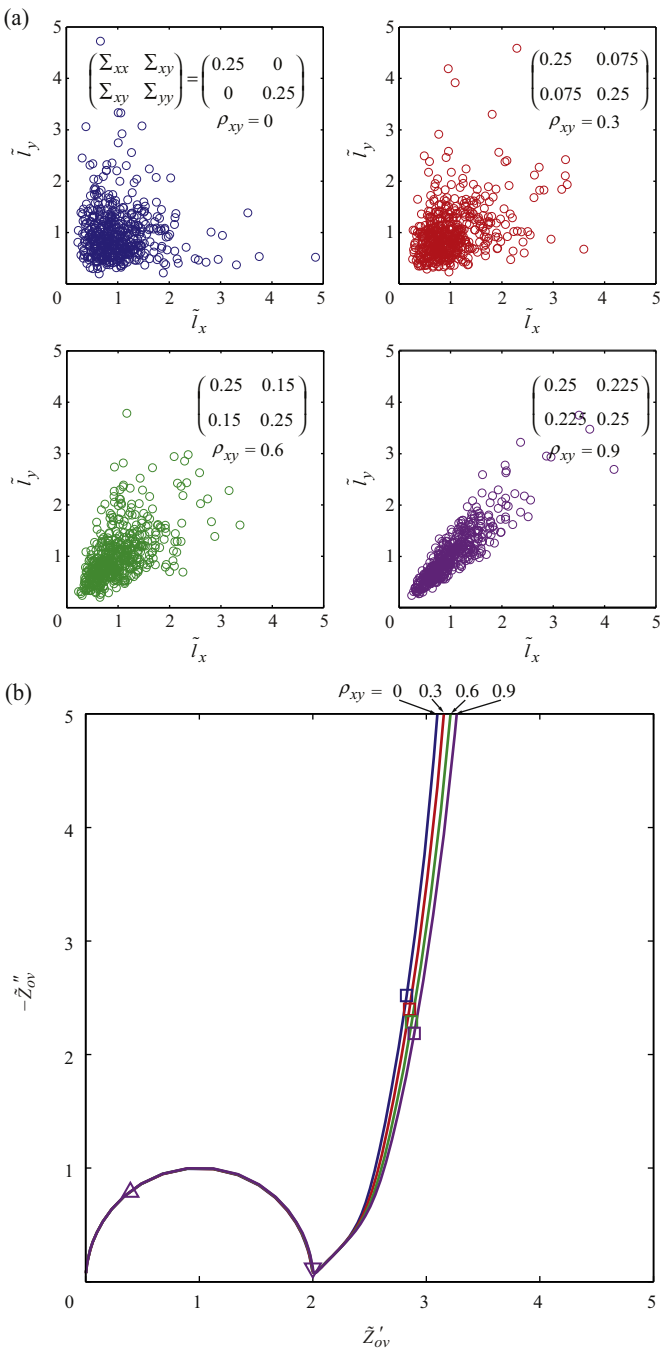

Fig. 8. (a) Correlated length distributions with various ρ_{xy} values, and (b) a complex plane plot of overall electrode impedance with the length distributions in (a). For each curve, △, ▽, and □ represent $\tilde{Z}_{ov}$ at $\tilde{\omega} = \chi_x$, χ_y, and 1, respectively. $\tilde{Z}_{ov}$ at $\tilde{\omega} = \tau$ raises out of the plot range.

and large $\tilde{l}_y$ are paired together, and small $\tilde{l}_x$ and small $\tilde{l}_y$ are paired together. Therefore, response of long diffusion lengths is weighted more by large insertion areas. Figure 8 (b) shows the behavior of $\tilde{Z}_{ov}$ in a complex plane, using the distributions in Figure 8 (a). As ρ_{xy} increases, the capacitive regime in diffusion impedance becomes more resistive and shifts in the positive real direction. This is because the response of long diffusion lengths is weighted heavier and presents a resistive contribution to the overall diffusion impedance.

Unlike the behavior of $\tilde{Z}_{ov}$ under uncorrelated length distributions, it is affected by the distribution in $\tilde{l}_y$, when the length distributions are correlated. Figure 9 (a) shows scattered plots of correlated length distributions with various Σ_{yy}, and constant Σ_{xx} and ρ_{xy}. Figure 9 (b) shows the behavior of $\tilde{Z}_{ov}$ on a complex plane, using the distributions in Figure 9 (a). As $\tilde{L}_y$ spreads wider with a larger Σ_{yy}, the capacitive regime in diffusion impedance becomes more resistive and shifts in the positive real direction. In fact, it turns out that the effect of increasing ρ_{xy} and the effect of increasing Σ_{yy} are very similar, given the lengths are correlated. When $\Sigma_{yy} > 0$ and $\rho_{xy} > 0$, $\tilde{L}_y$ spreads wider given a larger $\tilde{l}_x$, compared to its distribution given a smaller $\tilde{l}_x$. Therefore, the response of long diffusion lengths is weighted by a wider distribution of $\tilde{L}_y$, and it provides a resistive contribution to the diffusion impedance.

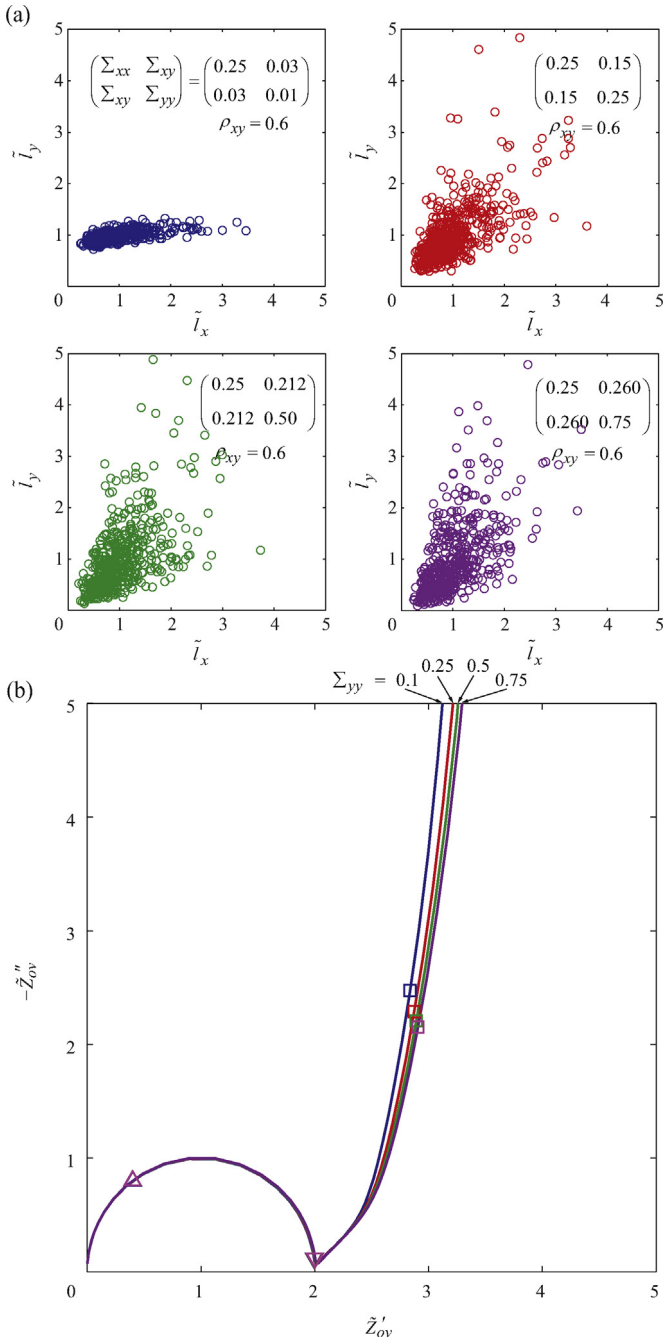

Fig. 9. (a) Correlated length distributions with various Σ_{yy} values, and (b) a complex plane plot of overall electrode impedance with the length distributions in (a). For each curve, △, ▽, and □ represent $\tilde{Z}_{ov}$ at $\tilde{\omega} = \chi_x$, χ_y, and 1, respectively. $\tilde{Z}_{ov}$ at $\tilde{\omega} = \tau$ raises out of the plot range.

5. Conclusion

In this article, impedance models were developed for an anisotropic battery particle and for an electrode consisting of such particles. Using the particle impedance model and typical parameter values, we studied the effects of anisotropies in various particle properties. It was found that the diffusion impedance may have various slopes in the Warburg regime when ion diffusion in the particle is anisotropic. The Warburg regime becomes more capacitive when one of the diffusivities increases, and more resistive when one of the diffusivities decreases. On the other hand, when the surface insertion kinetics and capacitance depend on the surface orientation, $\tilde{R}_p$ becomes a harmonic average of the charge transfer resistances, and $\tilde{C}_p$ becomes an arithmetic average of the surface capacitances. Thus, the RC transition frequency in particle impedance varies according to the change in $\tilde{R}_p$ and $\tilde{C}_p$. The diffusion impedance is also affected by the anisotropy in surface kinetics and approaches its 1D limits when one of the surfaces become relatively inactive.

Additionally, the effects of anisotropic length distributions were examined using the overall impedance model. It is assumed that the active particles in the electrode have strong anisotropies both in surface kinetics and bulk diffusion, which make the transport of ions effectively one-directional. The main diffusion length and the main insertion area were defined. When the two lengths are distributed independently, only the distribution in main diffusion length affects the diffusion impedance, making its capacitive regime inclined. If the length distributions are correlated, it is likely that the response of long diffusion lengths is weighted more by large insertion areas. It therefore raises a resistive contribution to the diffusion impedance. The resistive contribution is more significant when the correlation is higher or when the variance in main insertion area is larger. The general models in this article can also be used to investigate distribution effects of any other anisotropic properties.

Acknowledgements

This work was partially supported by a grant from the Samsung-MIT Alliance and by a fellowship to JS from the Kwanjeong Educational Foundation.

Appendix A. Nomenclature

Fourier transforms are denoted by a caret (□̂), and dimensionless variables are denoted by a tilde (□̃) [16,57]. This is different from the notation in some of the cited literatures[17,23,53] where the caret refers to model values in regression and the tilde refers to oscillating components.

Appendix B. Solution for the 2D anisotropic transport problem [54]

Ion diffusion in an anisotropic 2D rectangular domain is governed by Equations (21). This boundary value PDE problem can be reformulated to have homogeneous boundary conditions, by shifting the solution by a unity.

$$\Theta = \hat{\tilde{c}} + 1 \tag{B.1}$$

Then, as depicted in Figure B.1, the governing PDE and boundary conditions for Θ become

$$\begin{aligned} i\tilde{\omega}\left(\Theta - 1\right) &= \frac{\partial^2\Theta}{\partial\tilde{x}^2} + \tau\frac{\partial^2\Theta}{\partial\tilde{y}^2}\\ \left.\frac{\partial\Theta}{\partial\tilde{x}}\right|_{\tilde{x}=1} &+ \beta_x\,\Theta\big|_{\tilde{x}=1} = 0\\ \left.\frac{\partial\Theta}{\partial\tilde{y}}\right|_{\tilde{y}=1} &+ \beta_y\,\Theta\big|_{\tilde{y}=1} = 0\\ \left.\frac{\partial\Theta}{\partial\tilde{x}}\right|_{\tilde{x}=0} &= 0\\ \left.\frac{\partial\Theta}{\partial\tilde{y}}\right|_{\tilde{y}=0} &= 0 \end{aligned} \tag{B.2}$$

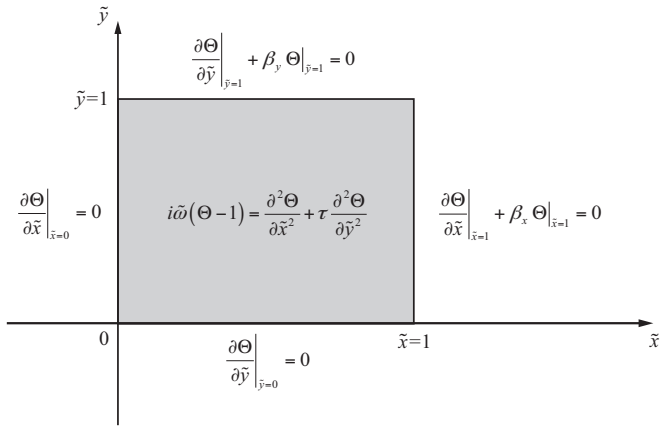

Fig. B.1. Dimensionless governing equation and boundary conditions for the 2D anisotropic ion transport problem.

Notice that the boundary conditions in Equations (B.2) are all homogeneous. In the FFT method, we hypothesize that the solution Θ can be written in a series expansion as

$$\Theta(\tilde{x},\tilde{y}) = \sum_{k}^{\infty} \Phi_k(\tilde{y})\,\Psi_k(\tilde{x}) \tag{B.3}$$

where Ψ_k are the basis functions, and Φ_k are the coefficient functions. Appropriate basis functions are

$$\Psi_k(\tilde{x}) = B_k\cos(\lambda_k\tilde{x}) \tag{B.4}$$

where

$$B_k = 2\sqrt{\frac{\lambda_k}{2\lambda_k+\sin(2\lambda_k)}} \tag{B.5}$$

and

$$\lambda_k\tan(\lambda_k) = \beta_x \tag{B.6}$$

for $0 < \lambda_k < \lambda_{k+1}$, and $k = 1, 2, 3, \ldots$.

In the FFT method, the PDE problem for Θ is transformed to a number of ordinary differential equation (ODE) problems for Φ_k for $k = 1, 2, 3, \ldots$, which is defined by Equation (B.3) or equivalently by

$$\Phi_k(\tilde{y}) = \left\langle \Psi_k(\tilde{x}),\,\Theta(\tilde{x},\tilde{y})\right\rangle = \int_0^1 \Psi_k(\tilde{x})\,\Theta(\tilde{x},\tilde{y})\,d\tilde{x} \tag{B.7}$$

Equations (B.2) are transformed by taking every terms in the equations inner product with Ψ_k.

$$\frac{d^2\Phi_k}{d\tilde{y}^2} - \left(\frac{i\tilde{\omega}+\lambda_k^2}{\tau}\right)\Phi_k + \frac{i\tilde{\omega}}{\tau}\left(\frac{B_k\sin(\lambda_k)}{\lambda_k}\right) = 0$$

$$\frac{d\Phi_k}{d\tilde{y}}\Big|_{\tilde{y}=1} + \beta_y\,\Phi_k\big|_{\tilde{y}=1} = 0 \tag{B.8}$$

$$\frac{d\Phi_k}{d\tilde{y}}\Big|_{\tilde{y}=0} = 0$$

The solution for this ODE problem is

$$\Phi_k(\tilde{y}) = \Gamma_k\left(1 - \frac{\beta_y\cosh(\Lambda_k\tilde{y})}{\beta_y\cosh(\Lambda_k)+\Lambda_k\sinh(\Lambda_k)}\right) \tag{B.9}$$

where

$$\Lambda_k = \sqrt{\frac{i\tilde{\omega}+\lambda_k^2}{\tau}} \tag{B.10}$$

and

$$\Gamma_k = \left(\frac{i\tilde{\omega}}{i\tilde{\omega}+\lambda_k^2}\right)\left(\frac{B_k\sin(\lambda_k)}{\lambda_k}\right) \tag{B.11}$$

The overall solution for $\Theta(\tilde{x},\tilde{y})$ then can be obtained by plugging the final expressions for $\Psi_k(\tilde{x})$ and $\Phi_k(\tilde{y})$ into Equation (B.3).

$$\Theta(\tilde{x},\tilde{y}) = \sum_{k=1}^{\infty}\Gamma_k\left(1 - \frac{\beta_y\cosh(\Lambda_k\tilde{y})}{\beta_y\cosh(\Lambda_k)+\Lambda_k\sinh(\Lambda_k)}\right)B_k\cos(\lambda_k\tilde{x}) \tag{B.12}$$

where λ_k, B_k, Λ_k and Γ_k are defined above. Finally we can shift Θ back by a negative unity to have the solution for $\hat{\tilde{c}}$.

$$\hat{\tilde{c}}(\tilde{x},\tilde{y}) = -1 + \sum_{k=1}^{\infty}\Gamma_k\left(1 - \frac{\beta_y\cosh(\Lambda_k\tilde{y})}{\beta_y\cosh(\Lambda_k)+\Lambda_k\sinh(\Lambda_k)}\right)B_k\cos(\lambda_k\tilde{x}) \tag{B.13}$$

This solution is employed in the main article and Appendix C, to calculate various impedance functions.

Appendix C. Particle impedance of the 2D rectangular particle

The integrals for $\tilde{Z}_p$ in Equation (23) can be performed separately. Expanding $\tilde{z}_{tot}$ on x normal surface,

$$\int_0^1\left(\tilde{z}_{tot}\big|_{\tilde{x}=1}\right)^{-1}d\tilde{y} = \int_0^1\left(\left(1+\tilde{z}_D\big|_{\tilde{x}=1}\right)^{-1} + \left(\tilde{z}_{acc}\big|_{\tilde{x}=1}\right)^{-1}\right)d\tilde{y} \tag{C.1}$$

where $\tilde{z}_{tot} = z_{tot}/\rho_{ct,x}$. Terms on the right hand side are

$$\tilde{z}_D\big|_{\tilde{x}=1} = \frac{z_D|_{\tilde{x}=1}}{\rho_{ct,x}} = \left(\frac{\partial\Delta\phi_{eq}}{\partial c}\right)\frac{\hat{c}\big|_{\tilde{x}=1}}{\rho_{ct,x}\hat{j}_{ins}\big|_{\tilde{x}=1}} = \frac{-\hat{\tilde{c}}\big|_{\tilde{x}=1}}{\hat{\tilde{c}}\big|_{\tilde{x}=1}+1} \tag{C.2}$$

and

$$\tilde{z}_{acc}\big|_{\tilde{x}=1} = \frac{z_{acc}|_{\tilde{x}=1}}{\rho_{ct,x}} = \frac{1}{i\omega C_{surf,x}\rho_{ct,x}} = \frac{\chi_x}{i\tilde{\omega}} \tag{C.3}$$

where $\chi_x = \omega_{RC,x}/\omega_{D,x}$. Plugging Equations (C.2) and (C.3) in Equation (C.1), we can analytically perform the integral.

$$\int_0^1\left(\tilde{z}_{tot}\big|_{\tilde{x}=1}\right)^{-1}d\tilde{y} = \int_0^1\left(\Theta\big|_{\tilde{x}=1} + i\tilde{\omega}/\chi_x\right)d\tilde{y}$$

$$= \left(\frac{i\tilde{\omega}}{\chi_x}\right) + \sum_{k=1}^{\infty}\Gamma_k\left(1 - \frac{\beta_y\sinh(\Lambda_k)}{\Lambda_k\beta_y\cosh(\Lambda_k)+\Lambda_k^2\sinh(\Lambda_k)}\right)B_k\cos(\lambda_k) \tag{C.4}$$

where λ_k, B_k, Λ_k, and Γ_k are defined in Appendix B for $k = 1, 2, 3, \ldots$.

The integral on y normal surface could be obtained through the similar method:

$$\int_0^1\left(\tilde{z}_{tot}\big|_{\tilde{y}=1}\right)^{-1}d\tilde{x} = \nu^{-1}\int_0^1\left(\Theta\big|_{\tilde{y}=1} + \left(i\tilde{\omega}/\tau\chi_y\right)\right)d\tilde{x}$$

$$= \frac{1}{\nu}\left(\left(\frac{i\tilde{\omega}}{\tau\chi_y}\right) + \sum_{k=1}^{\infty}\Gamma_k\left(\frac{\Lambda_k\sinh(\Lambda_k)}{\beta_y\cosh(\Lambda_k)+\Lambda_k\sinh(\Lambda_k)}\right)\left(\frac{B_k\sin(\lambda_k)}{\lambda_k}\right)\right) \tag{C.5}$$

where $\nu = \left(\rho_{ct,y}/\rho_{ct,x}\right)$, $\tau = \omega_{D,y}/\omega_{D,x}$, and $\chi_y = \omega_{RC,y}/\omega_{D,y}$. Putting the results together intoEquation (23), the particle

impedance has the following expression:

$$\tilde{Z}_p^{-1} = \left(\frac{i\tilde{\omega}}{2}\right)\left(\frac{1}{\chi_x}+\frac{\gamma}{\nu\tau\chi_y}\right) + \frac{1}{2}\sum_{k=1}^{\infty}\Gamma_k B_k\left(\cos(\lambda_k)+\frac{\left(\frac{\gamma\Lambda_k}{\nu\lambda_k}\right)\sinh(\Lambda_k)\sin(\lambda_k)-\beta_y sinh(\Lambda_k)\cos(\lambda_k)}{\Lambda_k\beta_y\cosh(\Lambda_k)+\Lambda_k^2\sinh(\Lambda_k)}\right) \quad (C.6)$$

This solution is employed in the main article to evaluate $\tilde{Z}_p$ and other related impedance functions.

Appendix D. The Gerischer limit of particle impedance

The Gerischer limit can be defined when the system has strongly anisotropic diffusion but relatively even surface insertion rate. It is also required that the charge transfer resistances are comparable to the largest diffusion characteristic resistance. In our system, such conditions are satisfied when $D_{ch,y} \gg D_{ch,x}$, $\nu \approx 1$, and $\beta_x \approx 1$. Under these conditions, the ion concentration varies much less in y direction compared to that in x direction, and we can approximate the concentration as a function of x only. The local variables can be replaced by their cross-sectional average along the y direction, which is defined as:

$$\hat{\bar{c}}(\tilde{x}) = \int_0^1 \hat{c}(\tilde{x},\tilde{y})\,d\tilde{y} \quad (D.1)$$

where $\hat{\bar{c}}$ is the cross-sectional average dimensionless concentration at a certain x. To obtain the governing equation for $\hat{\bar{c}}$, take the average of each term in Equations (21).

$$\frac{d^2\hat{\bar{c}}}{d\tilde{x}^2} = \left(i\tilde{\omega}+\tau\beta_y\right)\hat{\bar{c}} + \tau\beta_y$$

$$-\beta_x^{-1}\left.\frac{d\hat{\bar{c}}}{d\tilde{x}}\right|_{\tilde{x}=1} = 1+\left.\hat{\bar{c}}\right|_{\tilde{x}=1} \quad (D.2)$$

$$\left.\frac{d\hat{\bar{c}}}{d\tilde{x}}\right|_{\tilde{x}=0} = 0$$

Instead of the second order partial derivative in y, we obtain two terms in the governing equation: a first-order term and a constant. Each of them functions like a first order reaction and a zeroth order reaction, respectively. We can therefore expect that the impedance response would contain a Gerischer impedance element, may be with modification due to the zeroth order reaction term. The solution for this ODE problem is

$$\hat{\bar{c}} = D\cosh(\zeta\tilde{x}) - \left(\frac{\tau\beta_y}{i\tilde{\omega}+\tau\beta_y}\right) \quad (D.3)$$

where

$$D = -\left(\frac{\beta_x}{\zeta\sinh(\zeta)+\beta_x\cosh(\zeta)}\right)\left(\frac{i\tilde{\omega}}{i\tilde{\omega}+\tau\beta_y}\right) \quad (D.4)$$

and

$$\zeta = \sqrt{i\tilde{\omega}+\tau\beta_y} \quad (D.5)$$

Only the charge accumulation is considered on y surface, and the transport response on x normal surface is defined as the local Gerischer impedance. Therefore from Equation (23), the particle impedance becomes

$$\tilde{Z}_{p,G} = \left(\frac{1}{2}\left(\left(1+\tilde{z}_G\big|_{\tilde{x}=1}\right)^{-1}+\left(\tilde{z}_{acc}\big|_{\tilde{x}=1}\right)^{-1}\right)+\frac{1}{2}\gamma\left(\tilde{z}_{acc}\big|_{\tilde{y}=1}\right)^{-1}\right)^{-1} \quad (D.6)$$

where $\tilde{Z}_{p.G}$ and $\tilde{z}_G$ are the dimensionless particle impedance and the dimensionless local Gerischer impedance, respectively. $\tilde{z}_G$ can be calculated using the definition of $\tilde{z}_D$:

$$\tilde{z}_G = \beta_x\frac{\left.\hat{\bar{c}}\right|_{\tilde{x}=1}}{\left.\left(d\hat{\bar{c}}/d\tilde{x}\right)\right|_{\tilde{x}=1}} = \frac{\beta_x}{\zeta}\coth(\zeta)+\left(\frac{\tau\beta_y}{i\tilde{\omega}}\right)\left(1+\frac{\beta_x\coth(\zeta)}{\zeta}\right) \quad (D.7)$$

Then, $\tilde{Z}_{p.G}$ becomes

$$\tilde{Z}_{p,G}^{-1} = \left(\frac{i\tilde{\omega}}{2}\right)\left(\frac{1}{\chi_x}+\frac{\gamma}{\nu\tau\chi_y}\right)+\frac{1}{2}\left[\left(1+\frac{\tau\beta_y}{i\tilde{\omega}}\right)\left(1+\frac{\beta_x\coth(\zeta)}{\zeta}\right)\right]^{-1} \quad (D.8)$$

where $\beta_x\coth(\zeta)/\zeta$ is the bounded Gerischer impedance element. The additional term in the prefactor, $\tau\beta_y/i\tilde{\omega}$, is attributed to the constant term in the governing equation, Equation (D.2).

References

[1] M. Levi, D. Aurbach, The Journal of Physical Chemistry B 101 (1997) 4641–4647.
[2] D. Aurbach, M.D. Levi, E. Levi, H. Teller, B. Markovsky, G. Salitra, U. Heider, L. Heider, Journal of The Electrochemical Society 145 (1998) 3024–3034.
[3] R. Ruffo, S.S. Hong, C.K. Chan, R.A. Huggins, Y. Cui, The Journal of Physical Chemistry C 113 (2009) 11390–11398.
[4] A. Dhanda, H. Pitsch, R. O'Hayre, Journal of The Electrochemical Society 158 (2011) B877–B884.
[5] X. Dominguez-Benetton, S. Sevda, K. Vanbroekhoven, D. Pant, Chemical Society Reviews 41 (2012) 7228–7246.
[6] X. Yuan, H. Wang, J. Colin Sun, J. Zhang, International Journal of Hydrogen Energy 32 (2007) 4365–4380.
[7] L. Yang, R. Bashir, Biotechnology advances 26 (2008) 135–150.
[8] S. Arndt, J. Seebach, K. Psathaki, H.-J. Galla, J. Wegener, Biosensors and Bioelectronics 19 (2004) 583–594.
[9] K. Jüttner, Electrochimica Acta 35 (1990) 1501–1508.
[10] A. Nishikata, Y. Yamashita, H. Katayama, T. Tsuru, K. Tanabe, H. Mabuchi, Corrosion Science 37 (1995) 2059–2069.
[11] A. Ocampo, M. Miranda-Hernandez, J. Morgado, J. Montoya, P. Sebastian, Journal of power sources 160 (2006) 915–924.
[12] H. Yuan, D. Guo, X. Qiu, W. Zhu, L. Chen, Journal of Power Sources 188 (2009) 8–13.
[13] C. Ho, I.D. Raistrick, R.A. Huggins, Journal of The Electrochemical Society 127 (1980) 343–350.
[14] J.E.B. Randles, Discussions of the Faraday Society 1 (1947) 11–19.
[15] W. Lai, F. Ciucci, Journal of The Electrochemical Society 158 (2011) A115–A121.
[16] J. Song, M.Z. Bazant, Journal of The Electrochemical Society 160 (2013) A15–A24.
[17] M. Doyle, J.P. Meyers, J. Newman, Journal of The Electrochemical Society 147 (2000) 99–110.
[18] M.D. Levi, D. Aurbach, The Journal of Physical Chemistry B 108 (2004) 11693–11703.
[19] M.D. Levi, D. Aurbach, Journal of Power Sources 146 (2005) 727–731.
[20] F. Ciucci, W., Lai, Electrochimica Acta, (2012).
[21] P. Gambhire, K.S. Hariharan, A. Khandelwal, V.S. Kumar, S.M. Kolake, D. Oh, S. Doo, Journal of The Electrochemical Society 161 (2014) A183–A193.
[22] E. Barsoukov, J. Kim, D. Kim, K. Hwang, C. Yoon, H. Lee, Journal of New Materials for Electrochemical Systems 3 (2000) 301–308.
[23] J.P. Meyers, M. Doyle, R.M. Darling, J. Newman, Journal of The Electrochemical Society 147 (2000) 2930–2940.
[24] R. Huang, F. Chung, E. Kelder, Journal of The Electrochemical Society 153 (2006) A1459–A1465.
[25] J. Bisquert, G. Garcia-Belmonte, P. Bueno, E. Longo, L. Bulhoes, Journal of Electroanalytical Chemistry 452 (1998) 229–234.
[26] K. Persson, V.A. Sethuraman, L.J. Hardwick, Y. Hinuma, Y.S. Meng, A. van der Ven, V. Srinivasan, R. Kostecki, G. Ceder, The Journal of Physical Chemistry Letters 1 (2010) 1176–1180.
[27] D. Morgan, A. Van der Ven, G. Ceder, Electrochemical and solid-state letters 7 (2004) A30–A32.
[28] A. Van der Ven, G., Ceder, Electrochemical and Solid-State Letters, 3 (2000) 301-304.
[29] A. Van der Ven, G. Ceder, Journal of Power Sources 97–98 (2001) 529–531.
[30] C. Ouyang, S. Shi, Z. Wang, X. Huang, L. Chen, Physical Review B 69 (2004) 104303.
[31] R. Malik, D. Burch, M. Bazant, G. Ceder, Nano Letters 10 (2010) 4123–4127.
[32] R. Amin, P. Balaya, J. Maier, Electrochemical and solid-state letters 10 (2007) A13–A16.
[33] M.D. Levi, D. Aurbach, Electrochimica Acta 45 (1999) 167–185.
[34] M.A. Vorotyntsev, A.A. Rubashkin, J.P. Badiali, Electrochimica Acta 41 (1996) 2313–2320.
[35] L. Wang, F. Zhou, Y.S. Meng, G. Ceder, Physical Review B 76 (2007) 165435.

[36] D.A. Cogswell, M.Z. Bazant, Acs Nano 6 (2012) 2215–2225.
[37] D.A. Cogswell, M.Z. Bazant, Nano Letters 13 (2013) 3036–3041.
[38] M.Z. Bazant, Accounts of Chemical Research 46 (2013) 1144–1160.
[39] G.K. Singh, G. Ceder, M.Z. Bazant, Electrochimica Acta 53 (2008) 7599–7613.
[40] G. Chen, X. Song, T.J. Richardson, Electrochemical and Solid-State Letters 9 (2006) A295–A298.
[41] A. Van der Ven, C. Marianetti, D. Morgan, G. Ceder, Solid State Ionics 135 (2000) 21–32.
[42] F. Zhou, C.A. Marianetti, M. Cococcioni, D. Morgan, G. Ceder, Physical Review B 69 (2004) 201101.
[43] M. Nishizawa, R. Hashitani, T. Itoh, T. Matsue, I. Uchida, Electrochemical and solid-state letters 1 (1998) 10–12.
[44] E. Hosono, T. Kudo, I. Honma, H. Matsuda, H. Zhou, Nano letters 9 (2009) 1045–1051.
[45] S. Ju, H. Peng, G. Li, K. Chen, Materials Letters 74 (2012) 22–25.
[46] S. Lee, Y. Cho, H.K. Song, K.T. Lee, J. Cho, Angewandte Chemie International Edition 51 (2012) 8748–8752.
[47] P. Zhang, D. Zhang, Q. Yuan, X. Ren, T.D. Golden, Solid State Sciences 13 (2011) 1510–1515.
[48] E. Barsoukov, J.R. Macdonald, Impedance spectroscopy: theory, experiment, and applications, 2nd ed., Wiley-Interscience, Hoboken, N.J, 2005.
[49] F. Munakata, T. Ito, Y. Ohsawa, M. Kawai, Journal of Materials Science Letters 21 (2002) 117–119.
[50] J. Jamnik, J. Maier, Physical Chemistry Chemical Physics 3 (2001) 1668–1678.
[51] W. Lai, S.M. Haile, Journal of the American Ceramic Society 88 (2005) 2979–2997.
[52] Y. Lu, C. Kreller, S.B. Adler, Journal of The Electrochemical Society 156 (2009) B513–B525.
[53] M.E. Orazem, B. Tribollet, Electrochemical impedance spectroscopy, Wiley.com, 2011.
[54] W.M. Deen, Analysis of Transport Phenomena (Topics in Chemical Engineering), Oxford University Press, New York, 1998.
[55] H.-K. Song, H.-Y. Hwang, K.-H. Lee, L.H. Dao, Electrochimica Acta 45 (2000) 2241–2257.
[56] H.-K. Song, Y.-H. Jung, K.-H. Lee, L.H. Dao, Electrochimica Acta 44 (1999) 3513–3519.
[57] F. Ciucci, Y. Hao, D.G. Goodwin, Physical Chemistry Chemical Physics 11 (2009) 11243–11257.